Progress in Organic Coatings 192 (2024) 108505

Contents lists available at ScienceDirect

Progress in Organic Coatings

journal homepage: www.elsevier.com/locate/porgcoat

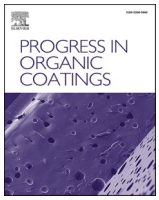

On the theoretical framework for meniscus-guided manufacturing of large-area OPV modules

Fabian Gumpert [a,*], Annika Janßen [a,b,c], Robin Basu [b], Christoph J. Brabec [b,c], Hans-Joachim Egelhaaf [b,c], Jan Lohbreier [a], Andreas Distler [b]

[a] Faculty of Applied Mathematics, Physics and Humanities, Nuremberg Institute of Technology OHM, Keßlerplatz 12, Nuremberg 90489, Bavaria, Germany
[b] Faculty of Engineering, Department of Material Science, Materials for Electronics and Energy Technology (i-MEET), Friedrich-Alexander-Universität, Erlangen-Nürnberg, Martensstraße 7, Erlangen 91058, Bavaria, Germany
[c] Helmholtz Institute Erlangen-Nürnberg for Renewable Energy (HI-ERN), Forschungszentrum Jülich GmbH, Immerwahrstraße 2, Erlangen 91058, Bavaria, Germany

ARTICLE INFO

Keywords:
Organic photovoltaics
Meniscus-guided coating
Analytical description
Thin films
Accelerated coating velocity
Computational fluid dynamics

ABSTRACT

For the manufacturing of thin films of solution-processable organic semiconductors, e.g. for organic photovoltaics (OPV), meniscus guided-coating techniques are the method of choice for large-scale industrial applications. However, the process requires an in-depth understanding of the respective fluid dynamics to control the resulting film thickness. In this article, we derive an analytical expression to describe the layer thickness of coatings manufactured with a trapezoidal-shaped applicator as a function of various fluid and process parameters. The analytical calculations are compared with results from computational fluid dynamics (CFD) simulations and experimental data for an industrially relevant OPV active material system. The good agreement of all three approaches demonstrates the potential of the analytical and simulative methods to minimize the number of time- and resource-consuming experiments. Furthermore, our theoretical model can be used to enhance the homogeneity of large-area coatings by means of an acceleration profile of the applicator that can compensate for the liquid loss during the coating process. The respective analytical expression is validated by simulated and experimentally obtained data for long-distance coatings. Finally, this approach is used to fabricate a large-area OPV module with new world record efficiency.

1. Introduction

The importance of photovoltaics has grown in recent years as the demand for renewable energy continues to increase. Solution-processable organic photovoltaics (OPV) receive more and more scientific and economical attention due to their unique characteristics, like light weight, high throughput, and semi-transparency [1]. The respective printing inks comprise the photoactive material dissolved in a solvent. After the deposition of the coating ink, the solvent evaporates during the drying process, leaving a dry film as the functional layer. Recent material developments result in photoelectric conversion efficiencies (PCEs) above 19 % [2–4] for small-scale cells (few mm^2) at laboratory level. Uniform and even layers with a predefined thickness are required to achieve these record efficiencies, since too thin layers lead to performance losses due to insufficient absorption, while too thick layers hamper charge extraction [5].

Solution-processable techniques are preferred processes for industrial applications, since they enable higher throughput (e.g. roll-to-roll manufacturing) and thus, lower costs. For roll-to-roll manufacturing, meniscus guided coating techniques are established methods to deposit the OPV materials [6–8]. Among these techniques, blade coating is scientifically and economically the most relevant technique, especially for the research on upscaling from small-scale cells to large-area modules. The upscaling to module size is still a major challenge that requires further investigation of the process [9]. Insufficient control and/or understanding of the deposition process results in uneven and non-uniform layer thicknesses and thus, to a decrease of the power conversion efficiency of the module.

In the blade coating process, an initial fluid volume is deposited between the applicator and the substrate to be coated. During the coating process, the applicator is moved horizontally and, by this, fluid is partially deposited onto the substrate. Consequently, the fluid volume beneath the applicator steadily decreases with coating distance. However, the fluid volume beneath the applicator influences the radius of the

* Corresponding author.
E-mail address: fabian.gumpert@th-nuernberg.de (F. Gumpert).

https://doi.org/10.1016/j.porgcoat.2024.108505
Received 30 January 2024; Received in revised form 23 April 2024; Accepted 29 April 2024
Available online 20 May 2024

down-stream meniscus, which is essential for the deposited wet film thickness [10]. As a consequence, the consumption of the fluid during the coating process leads to an uneven film thickness, i.e. an initially thicker film that becomes gradually thinner with coating distance, as shown in Fig. 1 or in the supplementary information (see Fig. S1 and Fig. S2).

Besides laboratory experiments, numerical simulation and analytical description are established methods to better understand the formation of the wet film and to optimize the deposition process. Moreover, simulation and theory approaches further decrease the number of time- and resource-expensive experiments. For example the influence of different blade geometries on the blade coating process are numerically investigated in [11]. CFD models are reported to investigate the blade coating process as a function of different variables (e.g. substrate speed and fluid properties) [12–14]. The theory of wet film formation is based on the work of Landau, Levich and Derjaguin [15,16]. Based on this theory, Gutenev et al. derived analytical expressions in [17] to further describe the blade coating process. According to the theory of wet film formation, the coating velocity can compensate for the fluid loss beneath the applicator. In [18,19], the influence of the coating velocity on the wet film thickness was experimentally investigated. In both articles, the theoretically predicted dependency of the film thickness on the coating velocity is confirmed. The consumption of the coating fluid results in a dynamic meniscus which was investigated in [20] with experimental, computational and analytical methods. In [10], we developed a numerical model of the coating process where the simulated thicknesses are in very good agreement with the experimental data. Furthermore, a linear function was derived which is able to predict the wet film thickness for a wide range of velocity and initial volume combinations.

In this article, we propose a complete theoretical framework for blade coating with a trapezoidal applicator shape, which does not only describe the influence of coating speed and ink volume, but also includes the ink properties, namely viscosity and surface tension.

In addition, for both the linear function of the previous work and the analytical formula, an expression is derived to describe an accelerated coating process to generate an even and uniform wet film with a constant targeted thickness. Finally, experiments are performed where the velocity of the applicator is increased according to the derived expressions. The resulting wet films provide a thickness as uniform as predicted and thus validate our simulations and analytical model. Thus, they prove to be powerful tools for all kinds of research and development using blade coating, e.g. OPV module production.

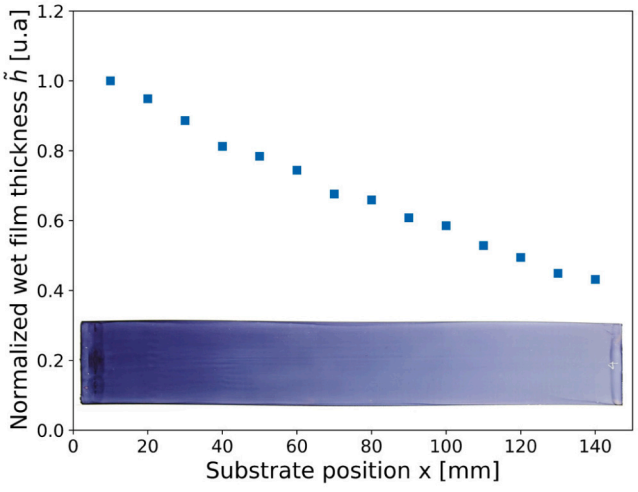

Fig. 1. Normalized thickness $\tilde{h}$ profile of a P3HT:O-IDTBR film, which is manufactured by blade coating with constant velocity (80 mm/s), over a coating distance of 15 cm and an initial volume of 60 μl. The steady decrease of film thickness from left to right can be observed in the experimentally obtained data points and is also clearly visible in the photograph of the respective sample.

2. Material and methods

2.1. Theoretical description of wet film thickness for trapezoidal applicator geometries

The theory of wet film formation dates back to the work of Landau-Levich [16] and Derjaguin [15]. In their work, they describe how the wet film is generated on a flat plate which is dragged out of a liquid (mixture of solvent and solute) reservoir. They assume a relatively fast coating velocity, so effects of the drying process can be neglected (Landau-Levich regime). Both articles propose an analytical expression for the generated wet film

$$h = 1.34 \cdot R \cdot Ca^{2/3}, \tag{1}$$

where h denotes the wet film thickness (SI-unit: m) and R the radius of the down-stream meniscus (SI-unit: m). The capillary number Ca is defined as

$$Ca = \frac{\mu \cdot u}{\sigma}, \tag{2}$$

where μ is the viscosity of the liquid (SI-unit: Pa·s), u is the velocity of the plate (SI-unit: m/s) and σ is the surface tension of the liquid in air environment (SI-unit: N/m). The theory was applied to meniscus-guided coating processes where cylindrical applicator geometries are used to predict the resulting wet film thickness [18,21].

It is found that the liquid volume beneath the applicator affects the radius of the down-stream meniscus and consequently also the resulting wet film thickness. Moreover, for cylindrical applicators also the angle between the applicator and the coating liquid varies with the volume, which makes the system even more complex. In contrast, applicators with trapezoidal-shaped tips provide constant angles between applicator and liquid as long as the volume is larger than a critical value. In [17], a tilted plate moves along a substrate. The gap between plate and substrate is filled with liquid. The authors derive an expression for the radius from fundamental geometrical considerations, if $h/R << 1$

$$R(S) = \sqrt{\frac{S}{\tan\left(\frac{\pi-\varphi}{2}\right) + \frac{\varphi-\pi}{2}}}. \tag{3}$$

Here, S denotes the cross-sectional area of the liquid (SI-unit: m^2) and φ the opening angle in radians between the substrate and the plate. In Fig. 2, the cross-sectional view of the coating process is shown and all

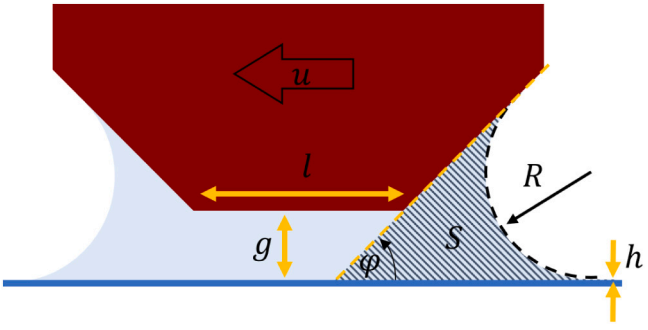

Fig. 2. Cross-sectional view of the meniscus-guided coating process. In the process, the coating liquid (light blue) is injected between the applicator tip (red) and the substrate (blue). The down-stream meniscus R, which mainly determines the wet film thickness, is indicated and is a function of the area S (hatched area). (For interpretation of the references to colour in this figure legend, the reader is referred to the web version of this article.)

relevant parameters for the calculation of the down-stream meniscus radius are indicated, apart from the applicator width w (SI-unit: m) that is orthogonal to the drawing plane.

The applicator moves with a velocity u at a constant height g over the substrate (SI-unit: m). Together with the length of the applicator tip l (SI-unit: m), a lower limit for the fluid volume can be calculated. The angle φ can be derived from the applicator geometry. Assuming a symmetrical liquid distribution beneath the applicator, which is valid for small velocities, the relevant liquid area S (SI-unit: m^2) can be derived from basic geometrical considerations

$$S(V) = \frac{\frac{g^2}{tan(\varphi)} + \frac{V}{w} - g \cdot l}{2}, \tag{4}$$

where V denotes the volume beneath the applicator (SI-unit: m^3). Inserting eqs. 2, 3, and 4 in 1, an analytical expression to predict the wet film thickness as a function of the coating velocity u and the volume V can be derived

$$h_{theo}(u, V) = 0.95 \sqrt{\frac{\left[\frac{g^2}{tan(\varphi)} + \frac{V}{w} - g \cdot l\right]}{tan\left(\frac{\pi-\varphi}{2}\right) + \frac{\varphi-\pi}{2}}} \left(\frac{\mu \cdot u}{\sigma}\right)^{2/3}. \tag{5}$$

2.2. The accelerated coating process for a constant film thickness

In a previous work [10], we presented a computational fluid dynamics (CFD) simulation as a digital twin of the coating process that only requires a few, experimentally easily accessible, liquid properties to predict the wet film thickness with good accuracy. Based on that, we derived a linear fit function to predict the wet film thickness

$$h_{fit}(u, V) = (b + c \cdot V) u^{2/3}, \tag{6}$$

where b and c are fit parameters which can be determined by the simulation results. The linear fit equation was developed for one specific experimental setup and is only valid for the utilized OPV material system and for an applicator width of 25 mm. However, by normalizing the parameter c with respect to the applicator width w $\left(c = \frac{c \cdot 25mm}{w} = \frac{\widetilde{c}}{w}\right)$, Eq. (6) is valid for arbitrary applicator widths

$$h_{fit}(u, V) = \left(b + \frac{\widetilde{c}}{w} \cdot V\right) u^{2/3}. \tag{7}$$

For OPV module-relevant coating distances (i.e. >10 cm), V will decrease considerably by the process itself. In general, the consumption of fluid during the coating process in x-direction can be expressed by

$$-\mathrm{d}V(x) = h(u, V) \cdot w \cdot \mathrm{d}x. \tag{8}$$

If a constant wet film thickness h_c is assumed, as it is desired for large-area coatings, Eq. (8) can be integrated

$$-\int_{V_0}^{V(x)} \mathrm{d}V(x) = \int_0^x h_c \cdot w \, \mathrm{d}x, \tag{9}$$

where V_0 is the initial fluid volume (SI-unit: m^3) at the starting position $x = 0$. In this case, the fluid volume beneath the applicator is a function of the coating distance x (SI-unit: m) and can be written as

$$V(x) = V_0 - h_c \cdot w \cdot x. \tag{10}$$

In both, Eq. (5) and Eq. (7), it can be seen that the wet film thickness is a function of the fluid volume and the velocity. Therefore, the loss of liquid during the coating process can be compensated for by gradually increasing the velocity of the applicator during the coating process, a technique that can easily be implemented. An expression $u_{theo}(x)$ to describe the required velocity at each position x can be derived from Eq. (5)

$$u_{theo}(x) = 1.08 \frac{\sigma}{\mu} \left\{ h_c \sqrt{\frac{tan\left(\frac{\pi-\varphi}{2}\right) + \frac{\varphi-\pi}{2}}{\left[\frac{g^2}{tan(\varphi)} + \frac{V_0}{w} - h_c \cdot x - g \cdot l\right]}} \right\}^{3/2}, \tag{11}$$

and a respective expression $u_{fit}(x)$ can be derived from Eq. (7)

$$u_{fit}(x) = \left[\frac{h_c}{b + \widetilde{c}\left(\frac{V_0}{w} - h_c \cdot x\right)}\right]^{3/2}. \tag{12}$$

2.3. Material system P3HT:O-IDTBR

Different experiments are carried out to validate the proposed accelerated coating approach. In all of these experiments, the material system P3HT:O-IDTBR is used which is based on the photoactive material combination of the donor polymer poly(3- hexylthiophene) (P3HT) and the non-fullerene acceptor (5Z,5′Z)-5,5′-((7,7′-(4,4,9,9-tetraoctyl-4, 9-dihydros- indaceno[1,2-b,5,6-b']dithiophene-2,7- diyl)bis (benzo [c][1,2,5]thiadiazole-7,4-diyl))bis(methanylylidene bis (3-ethyl-2-thioxothiazolidin-4-one))) (O-IDTBR). The material system offers good processing and stability properties [22,23] and thus, has a high relevance for large-area industrial OPV applications. In our previous work [10], we experimentally determined the different fluid-related properties of P3HT:O-IDTBR (dynamic viscosity μ, surface tension σ, and the contact angles with the applicator α and the glass substrate β) which are required for both the numerical simulation and the theoretical approach. Further information about the material system can be found in our previous paper.

3. Results and discussion

3.1. Comparison of theory, simulation, and experiment

In [10], experiments are performed to determine the wet film thickness of a blade-coated P3HT:O-IDTBR layer as a function of V_0 and u. The developed CFD simulation is shown to reproduce the experimental results with high precision. In Fig. 3, we compare these experimental and simulated results with calculations from our newly derived analytical expression (Eq. (5)).

Overall, the theoretical prediction shows excellent agreement with the simulation and experimental results. For velocities below 50 mm/s, a maximal difference between simulated and theoretically predicted wet film thickness of ~0.5 µm is obtained. For faster coating velocities, the theoretically calculated wet film thicknesses slightly differs from

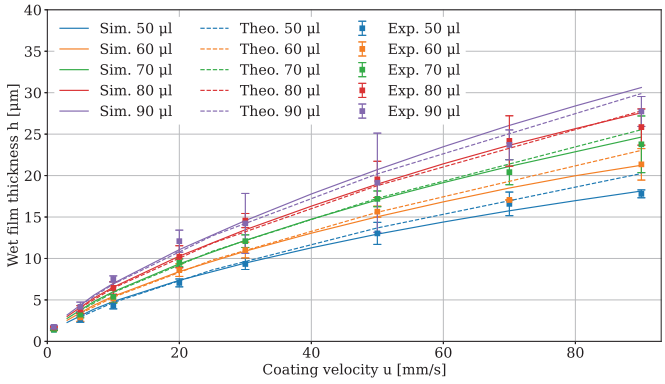

Fig. 3. Theoretically predicted according to Eq. (5) (dashed lines), simulated with CFD (solid lines), and experimentally measured (squares with corresponding error bars) wet film thicknesses as a function of the coating velocity for different initial liquid volumes.

simulation and experimental results. For such high velocities, the assumption of a symmetrically distributed liquid volume beneath the applicator (as shown in Fig. 2) has been shown not to be fulfilled anymore [10]. The meniscus is dragged more to the down-stream side, which can explain the differences in wet film thickness obtained by the different investigation methods. Photographs from the experiment confirm this explanation (see Fig. 4).

If the applicator is at rest (Fig. 4 a)), the coating fluid is symmetrically distributed beneath the applicator, whereas a unsymmetrical fluid distribution can be observed for a coating velocity of 90 mm/s (Fig. 4 b)). In the supplementary information, we provide more information about the asymmetry of the fluid distribution (see Fig. S3 and S4).

The results clearly confirm the validity of our theoretical model, which has been specially adapted to the geometry and physics of our system of investigation.

3.2. Influence of fluid parameters on the wet film thickness

In [10], all simulations and experiments are performed with the same coating fluid, namely a P3HT:O-IDTBR ink, which is an established material for the active layer in OPV. The material is assumed to be a incompressible Newtonian fluid, for which the surface tension and viscosity have been determined experimentally, since these are crucial fluid parameters for the coating process and the respective simulation. However, the development of novel materials for OPV is a current and very active research topic [9]. The creation of a large variety and number of new materials aims at further pushing the power conversion efficiency [3,4] or to improve the long-term stability of the active material [24,25]. However, each new material provides different fluid properties impacting the wet film thickness.

Therefore, our proposed simulation/theory approach is tested with respect to its flexibility regarding variation of fluid properties in the following. In Fig. 5, the theoretical and simulated results for an initial volume V_0 of 80 µl are shown. The wet film thicknesses are determined for different viscosities (Fig. 5 a)) and surface tensions of the fluid (Fig. 5 b)) by numerical simulations and the analytical expression.

In Fig. 5 a), results from the CFD simulation and the theory for velocities are very consistent for velocities below 50 mm/s. For faster coating velocities, the theory predicts slightly higher thicknesses compared to the simulation. This can again be explained by an asymmetrical fluid distribution under the applicator. For the dependence on the surface tension of the fluid, numerical simulation and analytical expression show an excellent agreement for all values of μ and σ (see Fig. 5 b)).

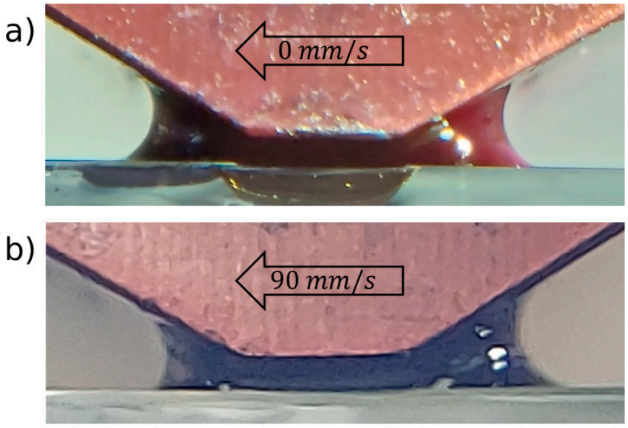

Fig. 4. Cross-sectional view of the experimental setup, where the tip of the applicator (red) and the coating ink (black) are visible. a) Symmetric fluid distribution, if the applicator is at rest (0 mm/s). b) Asymmetric fluid distribution, if the applicator moves with high coating velocity (90 mm/s). (For interpretation of the references to colour in this figure legend, the reader is referred to the web version of this article.)

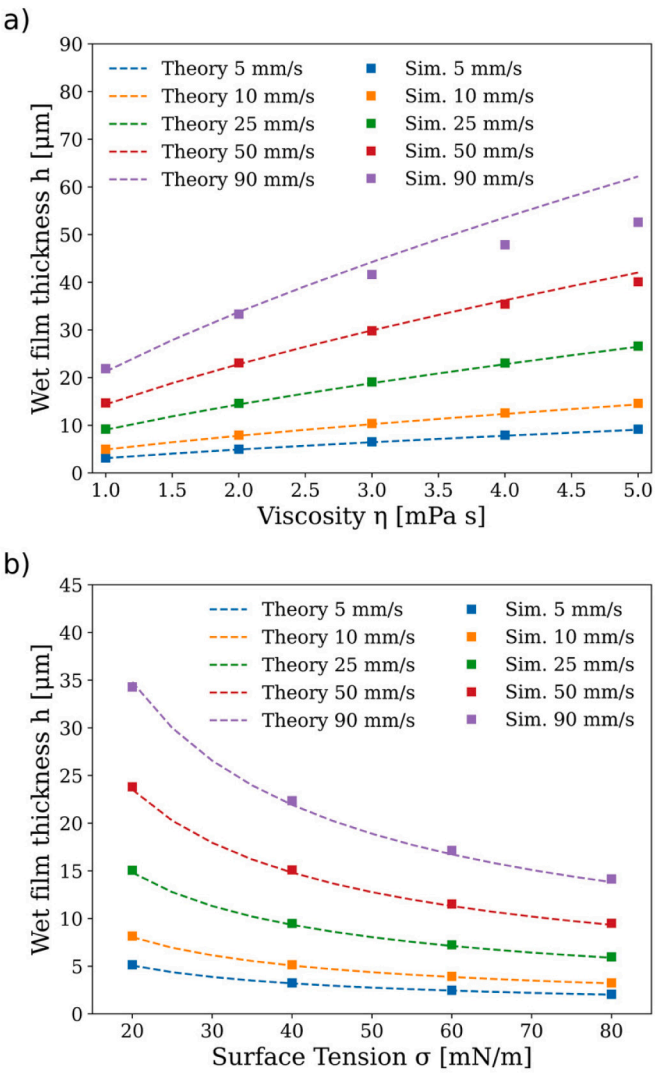

Fig. 5. The wet film thickness is plotted as a function of viscosity μ (a)) and surface tension σ (b)) for an initial liquid volume V_0 of 80 µl for different coating speeds u. In both a) and b), square markers indicate results from the CFD simulation and the theoretical calculations (Eq. (5)) are plotted as dashed lines.

Our CFD simulation model as well as our adapted theoretical function, provide the same results regarding variations in fluid properties. This strongly suggests that these results also match the real experimental findings. Thus, it can be used to predict and manipulate the coating thickness, as will be shown in the following chapter.

In the supplementary information, a similar figure to Fig. 5 can be found for an initial volume V_0 of 70 µl (see Fig. S5).

3.3. Homogeneous wet films processed by accelerated coating

For the investigation and implementation of an accelerated coating strategy, we used a Zehntner ZAA 2300 blade coating device that was electrically modified by Automatic Research GmbH to enable the pre-programming of a time-dependent speed profile $u(t)$. The velocity of the applicator u can be changed every 100 ms. As a consequence, we can apply our proposed fluid-specific acceleration strategy to compensate for the steadily decreasing film thickness upon coating due to the constant loss of fluid volume. Thus, the steadily decreasing film thickness could be compensated for by using a fluid-specific acceleration profile.

To apply the compensation strategy, the previous equations need to be reformulated to describe the velocity as a function of time. In general, the velocity of the applicator is the derivative of its position with respect to time. This approach, $dt = \frac{1}{u(x)}dx$, holds for both Eq. (11) and Eq. (12). Integrating this general equation over x and t results in an expression to describe the applicator position x as a function of t. This $x(t)$ can then be inserted into Eq. (11) or Eq. (12) again.

In the case of the theoretically derived equations, $u_{\mathrm{theo}}(t)$ can be written as

$$u_{\mathrm{theo}}(t) = 1.08\frac{\sigma}{\mu}\cdot h_c^{3/2} \cdot \left\{ \frac{\tan\left(\frac{\pi-\varphi}{2}\right)+\frac{\varphi-\pi}{2}}{\left[\left(\frac{g^2}{\tan(\varphi)}+\frac{V_0}{w}-g\cdot l\right)^{7/4} - 1.9\frac{t\cdot\sigma\cdot h_c^{5/2}\left(\tan\left(\frac{\pi-\varphi}{2}\right)+\frac{\varphi-\pi}{2}\right)^{3/4}}{\mu}\right]^{4/7}} \right\}^{3/4}. \tag{13}$$

An almost equivalent, but more compact, equation can be derived from the fit function approach

$$u_{\mathrm{fit}}(t) = \left\{ \frac{h_c}{\left[\left(b+\tilde{c}\frac{V_0}{w}\right)^{5/2} - 2.5\cdot\tilde{c}\cdot h_c^{5/2}\cdot t\right]^{2/5}} \right\}^{3/2}. \tag{14}$$

With these equations, the necessary velocities for a coating process with constant thickness h_c can be calculated and the respective time-velocity tables can be programmed in the device. For three different initial volumes V_0 (70, 80, and 90 µl) and a targeted constant wet film thickness h_c of 10 µm the time-velocity tables are calculated with the fully theoretical- (Eq. (13)) and the fit function- (Eq. (14)) approach. The resulting velocity profiles are shown in the following figure as a function of the corresponding substrate position x (Fig. 6).

For all initial volumes V_0, the velocity profiles, based on theoretical considerations and on the fit function, show some differences. The reason for the discrepancies can be seen in Fig. 3: Each approach predicts a slightly different velocity to manufacture a 10 µm thick wet film e.g. for an initial volume of 90 µl.

For the experimental validation of the accelerated coating strategy, the coating velocities for three different initial volumes (70, 80, and 90 µl) are calculated with Eq. (14). In Fig. 7, a photograph of a substrate after the drying process is shown. The accelerated coating strategy was applied to create a uniform wet film thickness of 10 µm onto the substrate, the initial volume of the coating ink was 90 µl.

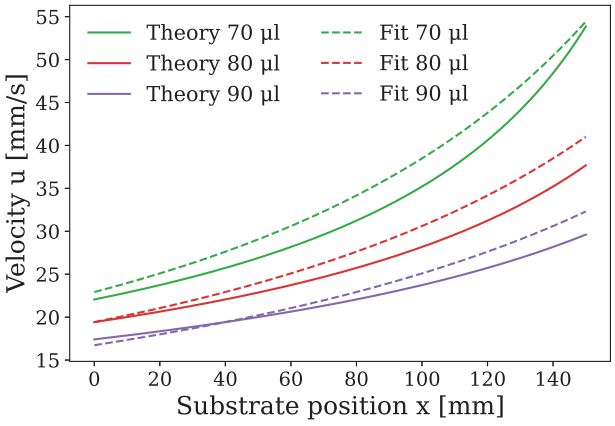

Fig. 6. The coating velocity u as a function of the substrate position is determined by the theoretical expression Eq. (11) (solid lines) and the fit function-approach Eq. (12) (dashed lines) for three different V_0 (70, 80, and 90 µl).

The dry film thicknesses are measured to validate the accelerated coating strategy. From the composition of the material system, we can conclude the wet film thickness from the dry film thickness [10]. The starting point of the measurements is 20 mm to exclude effects of the initial movement of the applicator on the film thickness. The thickness of the coating is measured every 10 mm until a coating distance of 110 mm has been reached. The respective calculated wet film thicknesses are plotted in Fig. 8 a) - c) (blue squares and error bars). CFD simulations are performed where the applicator acceleration is determined once with the theoretical expression (Eq. (13)) and once with the formula, which is based on the fit function (Eq. (14)). The results of the CFD simulations are plotted in Fig. 8 a) - c) as green dashed and purple dash-dotted lines for the theoretical- and fit function-approaches, respectively. Both approaches result in almost identical simulated wet film thicknesses. According to the CFD simulation, the acceleration, which is based on theoretical considerations, leads to slightly thicker wet films compared to the acceleration, according to Eq. (14). Note the adjustment of the y-axis limits to increase distinguishability of the individual data sets in the Fig. 8 a) - c).

These data prove that our simulative model and our analytical equation can be used to create a full set of process parameters. Both can easily be applied in practice to fabricate homogeneous coating over large distances.

In fact, we already implemented this approach very recently into the manufacturing process of high-performance large-area OPV modules, which enabled us to yield a new world record efficiency for OPV modules with 14.5 % on 204 cm^2 [26]. In [27], we reported on manufacturing of the large-area module with focus on the experimental details. The world record module is depicted in Fig. 9 and demonstrates the excellent film homogeneity over the whole module area (<5 % from the targeted dry film thickness 128 nm), which is crucial for its high power conversion efficiency.

It is to note that a respective module, whose active layer was coated with constant velocity and thus shows a strong thickness gradient, yields a PCE that is ~ 18 % lower, relative to a module fabricated by accelerated blade coating.

4. Conclusion

In this article, we derived a theoretical expression to predict the height of the deposited wet film in the doctor blading process. The predicted wet film thickness of the theoretical description was compared to experimental data and results of a corresponding CFD simulation. Overall, the investigated cases – including variations of the ink's viscosity and surface tension – show excellent agreement. Thus, both the proposed theoretical description and the simulation model allow for an extremely time- and resource-efficient approach to high-throughput research. Its flexibility is crucial for areas of application like OPV manufacturing, where a large number of novel materials is tested on a very short time scale.

Fig. 7. Photograph of a P3HT:O-IDTBR film deposited with accelerated balde coating using 90 µl initial volume. The coating direction x is indicated as well as the regarding distance from the coating start point ($x = 0$ mm).

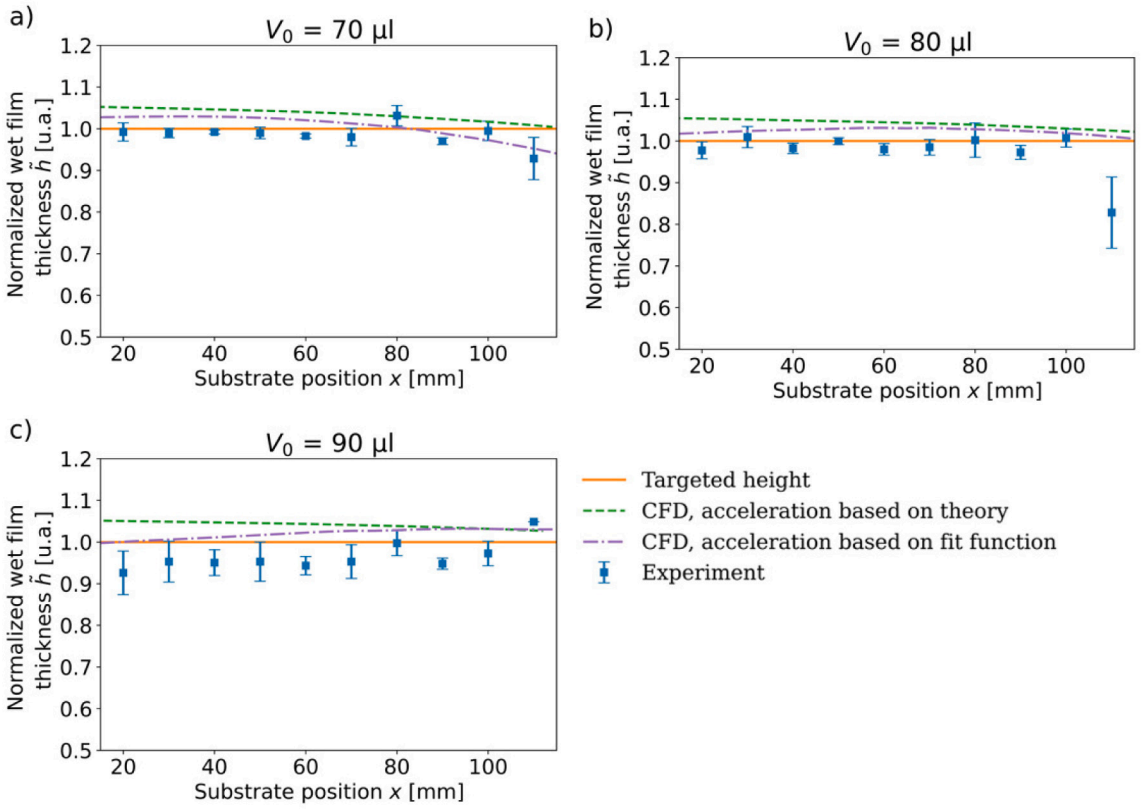

Fig. 8. a) - c) Normalized wet film thicknesses for initial volumes 70 µl, 80 µl, and 90 µl, respectively. Experimentally determined wet film thicknesses are indicated as blue squares with error bars, averaged over two samples per variation. CFD results, which are based on the acceleration strategy according to Eq. (13) and to Eq. (14) are plotted as green dashed lines and purple dash-dotted lines, respectively. All thicknesses are normalized with respect to the targeted wet film thickness of 10 µm (solid orange line).

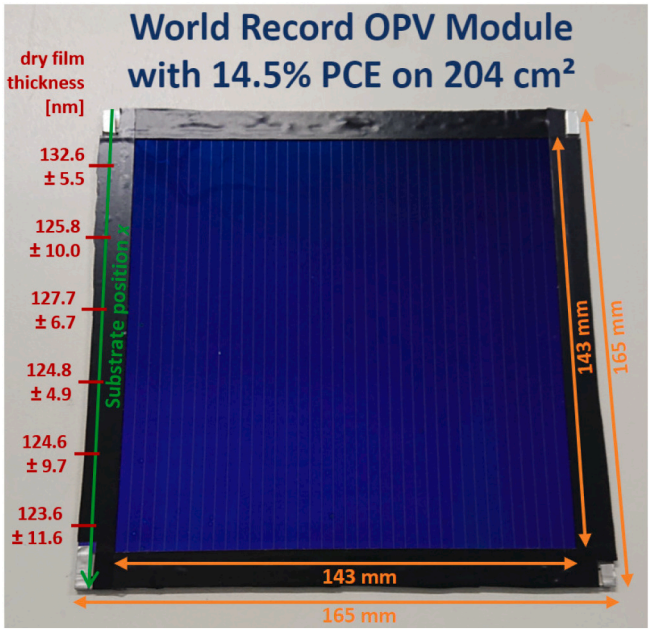

Fig. 9. Photograph of the organic photovoltaic (OPV) module with a new world record power conversion efficiency (PCE) of 14.5 % on 204 cm^2 enabled by accelerated blade coating. The OPV module was manufactured on a 165 mm × 165 mm substrate, with an aperture area of 143 mm × 143 mm. The dry film thickness was determined at six different vertical substrate positions x along the coating direction, each value being an average over six measurements at different horizontal positions.

Furthermore, these results have enabled us to derive expressions for an optimal applicator velocity profile which produces uniform layers with predefined thickness. This acceleration strategy was experimentally validated for long coating distances: Experiment, simulation, and calculation yield similar heights all of which are close to the targeted thickness.

For batch-to-batch production (e.g. direct coating onto silicon wafers for the fabrication of multi-junction solar modules), the accelerated coating process is an industrially highly relevant coating technique. In comparison with batch-to-batch slot-die coating, the advantages of accelerated blade coating are, on one hand, a smaller ink consumption (no large "dead volume" as inside syringes, tubes, and dies), and, on the other hand, a controlled film thickness right from the beginning of the coating (whereas for slot die coating the interplay of flow rate and coating speed usually requires some initial time/distance to form a stable steady-state meniscus of defined volume that is needed to form a homogeneous film). Continuous blade coating with fluid injection and slot-die coating are the analogous coating techniques to be used in a respective roll-to-roll manufacturing, where large-area coatings are generated on flexible substrates. The fluid-dynamic investigations and simulations presented in this work can also be adapted to such continuous coating processes.

This newly developed technique was ultimately applied to fabricate uniform large area coatings for high-performance organic solar modules. Finally, it allowed us to achieve a new world record for OPV module efficiency proving the importance and applicability of this work.

CRediT authorship contribution statement

Fabian Gumpert: Writing – review & editing, Writing – original draft, Visualization, Methodology, Investigation. **Annika Janßen:**

Writing – review & editing, Validation, Investigation. **Robin Basu:** Writing – review & editing, Validation. **Christoph J. Brabec:** Writing – review & editing, Resources. **Hans-Joachim Egelhaaf:** Writing – review & editing, Resources. **Jan Lohbreier:** Writing – review & editing, Supervision, Conceptualization. **Andreas Distler:** Writing – review & editing, Supervision, Conceptualization.

Declaration of competing interest

The authors declare no competing financial interest or personal relationship that could have appeared to influence the work reported in this paper.

Data availability

Data will be made available on request.

Acknowledgements

This work was supported by the Bavarian State Ministry for Science and Art via the Energy Campus Nürnberg (EnCN) and the European Union's Horizon 2020 research and innovation program [Grant numbers 952911 and 101007084].

Appendix A. Supplementary data

Supplementary data to this article can be found online at https://doi.org/10.1016/j.porgcoat.2024.108505.

References

[1] Hu Yingyue, Jiayu Wang, Cenqi Yan, Pei Cheng, The multifaceted potential applications of organic photovoltaics, Nat. Rev. Mater. 7 (11) (September 2022) 836–838, https://doi.org/10.1038/s41578-022-00497-y.

[2] Rui Sun, Wu Yao, Xinrong Yang, Yuan Gao, Zeng Chen, Kai Li, Jiawei Qiao, Tao Wang, Jing Guo, Chao Liu, Xiaotao Hao, Haiming Zhu, Jie Min, Single-junction organic solar cells with 19.17% efficiency enabled by introducing one asymmetric guest acceptor, Adv. Mater. 34 (26) (May 2022), https://doi.org/10.1002/adma.202110147.

[3] Lingling Zhan, Shuixing Li, Yaokai Li, Rui Sun, Jie Min, Zhaozhao Bi, Wei Ma, Zeng Chen, Guangqing Zhou, Haiming Zhu, Minmin Shi, Lijian Zuo, Hongzheng Chen, Desired open-circuit voltage increase enables efficiencies approaching 19% in symmetric-asymmetric molecule ternary organic photovoltaics, Joule 6 (3) (March 2022) 662–675, https://doi.org/10.1016/j.joule.2022.02.001.

[4] Lei Zhu, Ming Zhang, Xu Jinqiu, Chao Li, Jun Yan, Guanqing Zhou, Wenkai Zhong, Tianyu Hao, Jiali Song, Xiaonan Xue, Zichun Zhou, Rui Zeng, Haiming Zhu, Chun-Chao Chen, Roderick C.I. MacKenzie, Yecheng Zou, Jenny Nelson, Yongming Zhang, Yanming Sun, Feng Liu, Single-junction organic solar cells with over 19% efficiency enabled by a refined double-fibril network morphology, Nat. Mater. 21 (6) (May 2022) 656–663, https://doi.org/10.1038/s41563-022-01244-y.

[5] Kanupriya Khandelwal, S. Shyam Shankar, Prateek Malhotra, Subhayan Biswas, Abhishek Panghal, Susanta Sinha Roy, Ganesh D. Sharma, Unraveling the impact of thickness on active layer morphology and device performance of semitransparent organic solar cells: a comprehensive study, ACS Appl. Energy Mater. 6 (19) (2023) 10078–10087, https://doi.org/10.1021/acsaem.3c01685.

[6] Stephane Berny, Nicolas Blouin, Andreas Distler, Hans-Joachim Egelhaaf, Michal Krompiec, Andreas Lohr, Owen R. Lozman, Graham E. Morse, Lana Nanson, Agnieszka Pron, Tobias Sauermann, Nico Seidler, Steve Tierney, Priti Tiwana, Michael Wagner, Henry Wilson, Solar trees: first large-scale demonstration of fully solution coated, semitransparent, flexible organic photovoltaic modules, Adv. Sci. 3 (5) (December 2015), https://doi.org/10.1002/advs.201500342.

[7] Gu Xiaodan, Yan Zhou, Gu Kevin, Tadanori Kurosawa, Yikun Guo, Yunke Li, Haoran Lin, Bob C. Schroeder, Hongping Yan, Francisco Molina-Lopez, Christopher J. Tassone, Cheng Wang, Stefan C.B. Mannsfeld, He Yan, Dahui Zhao, Michael F. Toney, Zhenan Bao, Roll-to-roll printed large-area all-polymer solar cells with 5% efficiency based on a low crystallinity conjugated polymer blend, Adv. Energy Mater. 7 (14) (March 2017), https://doi.org/10.1002/aenm.201602742.

[8] W.T.N.G. Leonard, Seok Woo Lee, Dong Wook Chang, Justin M. Hodgkiss, Doojin Vak, Organic photovoltaics' new renaissance: advances toward roll-to-roll manufacturing of non-fullerene acceptor organic photovoltaics, Adv. Mater. Technol. 7 (10) (February 2022), https://doi.org/10.1002/admt.202101556.

[9] Guichuan Zhang, Francis R. Lin, Feng Qi, Thomas Heumüller, Andreas Distler, Hans-Joachim Egelhaaf, Ning Li, Philip C.Y. Chow, Christoph J. Brabec, Alex K.-Y. Jen, Hin-Lap Yip, Renewed prospects for organic photovoltaics, Chem. Rev. 122 (18) (2022) 14180–14274, https://doi.org/10.1021/acs.chemrev.1c00955.

[10] Fabian Gumpert, Annika Janßen, Christoph J. Brabec, Hans-Joachim Egelhaaf, Jan Lohbreier, Andreas Distler, Predicting layer thicknesses by numerical simulation for meniscus-guided coating of organic photovoltaics, Eng. Appl. Comput. Fluid Mech. 17 (1) (2023), https://doi.org/10.1080/19942060.2023.2242455.

[11] Ilias Iliopoulos, L.E. Scriven, A blade-coating study using a finite-element simulation, Phys. Fluids 17 (12) (December 2005), https://doi.org/10.1063/1.2140226.

[12] Evan Mitsoulis, George Athanasopoulos, Numerical simulation of blade-over-roll coating forming flows, Comput. Methods Mater. Sci. 10 (4) (2010) 214–224.

[13] Markus Schmidt, Uwe Schloßer, Eckhard Schollmeyer, Computational fluid dynamics investigation of the static pressure at the blade in a blade coating process, Text. Res. J. 79 (7) (May 2009) 579–584, https://doi.org/10.1177/0040517508093440.

[14] Arpan R. Singh, Scott J. Ormiston, Cfd analysis of blade coating from a reservoir onto a horizontal substrate using a homogeneous two-phase model, Can. J. Chem. Eng. 100 (2) (2021) 349–362, https://doi.org/10.1002/cjce.24096.

[15] B. Derjaguin, On the thickness of the liquid film adhering to the walls of a vessel after emptying, Prog. Surf. Sci. 43 (1–4) (1993) 134–137, https://doi.org/10.1016/0079-6816(93)90022-n.

[16] L. Landau, B. Levich, Dragging of a liquid by a moving plate, Dynam. Curved Fronts (1988) 141–153, https://doi.org/10.1016/b978-0-08-092523-3.50016-2.

[17] P.I. Gutenev, A.M. Pyatnitskii, N.V. Klimova, Liquid entrainment from the meniscus of a liquid wedge by a moving horizontal plate, Colloid J. 65 (3) (2003) 301–304, https://doi.org/10.1023/a:1024246520784.

[18] Byoungchoo Park, Mi-young Han, Photovoltaic characteristics of polymer solar cells fabricated by pre-metered coating process, Opt. Express 17 (16) (2009) 13830, https://doi.org/10.1364/oe.17.013830.

[19] Pei-Ting Tsai, Yu Kai-Chieh, Chia-Ju Chang, Sheng-Fu Horng, Hsin-Fei Meng, Large-area organic solar cells by accelerated blade coating, Org. Electron. 22 (2015) 166–172, https://doi.org/10.1016/j.orgel.2015.03.001.

[20] Hyungjoo Yim, Jaewook Nam, Analysis of low-speed blade coating flows, J. Fluid Mech. 978 (2024), https://doi.org/10.1017/jfm.2023.991.

[21] Felix Nickel, Christian Sprau, Michael F.G. Klein, Panagiota Kapetana, Nico Christ, Xin Liu, Soenke Klinkhammer, Uli Lemmer, Alexander Colsmann, Spatial mapping of photocurrents in organic solar cells comprising wedge-shaped absorber layers for an efficient material screening, Sol. Energy Mater. Sol. Cells 104 (2012) 18–22, https://doi.org/10.1016/j.solmat.2012.04.026.

[22] Ardalan Armin, Wei Li, Oskar J. Sandberg, Zuo Xiao, Liming Ding, Jenny Nelson, Dieter Neher, Koen Vandewal, Safa Shoaee, Tao Wang, Harald Ade, Thomas Heumüller, Christoph Brabec, Paul Meredith, A history and perspective of non-fullerene electron acceptors for organic solar cells, Adv. Energy Mater. 11 (15) (2021), https://doi.org/10.1002/aenm.202003570.

[23] S. Strohm, F. Machui, S. Langner, P. Kubis, N. Gasparini, M. Salvador, I. McCulloch, H.-J. Egelhaaf, C.J. Brabec, P3ht: non-fullerene acceptor based large area, semi-transparent pv modules with power conversion efficiencies of 5 processed by industrially scalable methods, Energy Environ. Sci. 11 (8) (2018) 2225–2234, https://doi.org/10.1039/c8ee01150h.

[24] Yan-Fu Liu, Si-Wen Zhang, Yan-Xun Li, Shi-Lin Li, Li-Qing Huang, Ya-Nan Jing, Qian Cheng, Lin-Ge Xiao, Bo-Xin Wang, Bing Han, et al., Solution-processed molybdenum oxide hole transport layer stabilizes organic solar cells, Chin. J. Polym. Sci. 41 (2) (2022) 202–211, https://doi.org/10.1007/s10118-022-2873-3.

[25] Kaihu Xian, Shengnan Zhang, Xu Ye, Junwei Liu, Kangkang Zhou, Zhongxiang Peng, Mingfei Li, Yu Wenchao Zhao, Zhuping Fei Chen, et al., Refining acceptor aggregation in nonfullerene organic solar cells to achieve high efficiency and superior thermal stability, SCIENCE CHINA Chem. 66 (1) (2022) 202–215, https://doi.org/10.1007/s11426-022-1394-y.

[26] Champion Photovoltaic Module Efficiency Chart — nrel.gov. https://www.nrel.gov/pv/module-efficiency.html, 2024 [Accessed 28-03-2024].

[27] Robin Basu, Fabian Gumpert, Jan Lohbreier, Pierre-Olivier Morin, Varun Vohra, Yang Liu, Yinhua Zhou, Christoph J. Brabec, Hans-Joachim Egelhaaf, Andreas Distler, Large-area organic photovoltaic modules with 14.5% certified world record efficiency, Joule (2024), https://doi.org/10.1016/j.joule.2024.02.016.